Advances in Aircraft and Spacecraft Science, *Vol. 12, No. 3 (2025) 197-216*
https://doi.org/10.12989/aas.2025.12.3.197

Coupled effects of fiber orientation and delamination on mechanical performance of composite laminates exposed to asymmetrical environmental conditions

Mohamed Khodjet Kesba*[1], B. Boukert[1a], A. Benkhedda[1b] and E.A. Adda Bedia[2c]

[1]*Aeronautical Sciences Laboratory*, *Institute of Aeronautics and Space Studies*, *University of Blida 1*, *BP 270 Route de Soumaa*, *Blida 09000*, *Algeria*
[2]*Laboratory of Materials and Hydrology*, *University of Sidi Bel Abbes*, *Sidi Bel Abbes*, *Algeria*

(Received April 17, 2025, Revised June 17, 2025, Accepted July 14, 2025)

Abstract. This study presents a coupled analytical approach to predict stiffness degradation in composite laminates affected by transverse cracking and delamination under asymmetrical environmental conditions. A modified shear-lag model incorporating both parabolic and progressive shear stress distributions is used to quantify relative and total stiffness loss. The theoretical framework builds on Classical Laminate Theory (CLT), extended to include stress perturbations and interface damage. This choice ensures compatibility with laminate-level mechanical behavior while enhancing local damage representation. Model predictions are validated against experimental data for T800H/3631 laminates, showing strong agreement across varying crack densities and temperatures. The results confirm that fiber orientation, delamination ratio, and environmental gradients significantly influence stiffness degradation. Compared to previous models based solely on CLT or simplified degradation factors, the present approach captures the interactive effects of damage and asymmetric moisture diffusion more realistically. These insights inform the design of more durable aerospace composite structures operating in harsh hygrothermal environments.

Keywords: angle ply; asymmetrical environment; delamination; diffusivity; stiffness

1. Introduction

Composite laminates are widely used in aerospace, automotive, and marine structures due to their high strength-to-weight ratio and tunable mechanical properties. However, their durability is significantly compromised when exposed to harsh hygrothermal environments, leading to progressive damage phenomena such as transverse cracking and interlaminar delamination. These degradation mechanisms are not only influenced by external conditions (e.g., temperature, humidity) but also by intrinsic parameters like fiber orientation, stacking sequence, and ply thickness. Traditionally, the analysis of damage in composite laminates has focused on isolated failure mechanisms, primarily transverse matrix cracking, as seen in the foundational work of

*Corresponding author, Ph.D., E-mail: mkhojet@gmail.com
[a]Ph.D., E-mail: bilanosky@hotmail.fr
[b]Professor, E-mail: aaminabenkhedda@gmail.com
[c]Professor, E-mail: addabed@yahoo.com

http://www.techno-press.org/?journal=aas&subpage=7 ISSN: 2287-528X (Print), 2287-5271 (Online)

Berthelot *et al*. (1996). While such studies have enhanced our understanding of crack initiation and density evolution, they fall short in capturing the synergistic interaction with delamination, which is particularly critical under asymmetrical environmental exposures.

Recent studies have advanced our understanding of delamination mechanics. For instance, Liu *et al.* (2025) conducted double cantilever beam (DCB) tests on CFRP laminates with various interface configurations and demonstrated that fracture toughness is dependent on both crack length and ply orientation. Similarly, Sheng *et al*. (2023) investigated the impact of nanoparticle and thermoplastic veil toughening on interlaminar fracture resistance under hygrothermal aging. While these works contribute valuable insights, they treat delamination as a standalone phenomenon, often neglecting the role of transverse cracks as precursors or accelerants of interlaminar separation.

Environmental exposure further complicates this picture. Multiple authors (e.g., Hanyu *et al.* 2023, Jing *et al*. 2023) have reported that long-term hygrothermal aging alters both the fiber-matrix interface and the resin phase, leading to a reduction in stiffness, toughness, and adhesion. For example, Behera *et al*. (2020, 2023) used nanoscale microscopy techniques to quantify interfacial debonding due to prolonged aging, showing that degradation is more pronounced in inner plies. These studies confirm that aging is not uniform across the laminate thickness, which makes symmetrical modeling assumptions problematic.

Furthermore, the interaction between damage progression and asymmetric environmental exposure remains insufficiently explored. Most analytical models, including those based on Classical Laminate Theory (CLT), assume symmetrical diffusion and ignore the dynamic feedback between mechanical degradation and diffusivity. Yet, recent studies (e.g., Wen 2023, Oshin *et al*. 2023) emphasize that cracked and delaminated zones act as moisture ingress facilitators, significantly accelerating aging kinetics. The work of Jayant *et al.* (2022), for example, linked delamination size to reduced aeroelastic performance in smart composite structures exposed to hygrothermal cycling, reinforcing the need to model these coupled effects.

Despite the breadth of literature, there remains a critical research gap: the lack of analytical models that can capture the combined influence of transverse cracks and delamination on stiffness degradation, particularly under asymmetrical environmental conditions. The existing frameworks often adopt simplified shear-lag assumptions or constant property degradation factors, which fail to reflect the evolving stress fields and moisture gradients. Moreover, very few models account for how environmental asymmetry modifies the delamination growth rate or alters the crack delamination interaction zone.

While (CLT) remains a foundational framework in composite mechanics, its assumptions particularly regarding through-thickness stress uniformity make it insufficient for accurately capturing interlaminar stresses, which are critical in the presence of transverse cracks and delamination. This limitation becomes more pronounced in laminates exhibiting strong through-thickness anisotropy or asymmetric environmental loading. To overcome these deficiencies, higher-order structural theories such as First-order Shear Deformation Theory (FSDT), Layerwise theories, and Zig-Zag models have been proposed in the literature (Reddy 2004, Carrera *et al*. 2011). These approaches improve the representation of interlaminar stress fields and deformation gradients, but often at the cost of increased computational complexity.

Recent efforts have also focused on capturing the coupled interaction between transverse cracks and delamination in thick composite laminates using advanced structural formulations. For instance, Lu *et al.* (2018) proposed an extended layerwise solid element hybrid method to simulate stiffened laminates with through-thickness damage, while Li *et al*. (2016) developed an enhanced

layerwise approach capable of modeling multiple delaminations and transverse cracks simultaneously. These studies confirm the need for refined structural theories to accurately represent localized damage mechanisms in thick or hybrid laminates. Our approach builds upon these insights by incorporating shear-lag-based stress perturbation functions into a CLT framework, offering a tractable alternative that captures key damage interactions without the computational burden of fully numerical models.

Some recent efforts, such as those by Khodjet-Kesba *et al.* (2016, 2019), Sereir *et al.* (2006), adopted enhanced shear-lag formulations that introduce stress perturbation functions into the CLT framework. This hybrid modeling strategy captures the nonlinear redistribution of stresses around cracks and delaminated zones while retaining the mathematical tractability of CLT. Moreover, it allows for analytical expressions of stiffness degradation that can be efficiently evaluated across a range of fiber orientations, ply thicknesses, and damage levels.

To address this gap, the present study proposes a refined shear-lag-based analytical model that integrates progressive and parabolic shear stress distributions, allowing simultaneous treatment of transverse cracking, delamination, and asymmetric hygrothermal diffusion. This model builds upon prior work (e.g., Khodjet-Kesba *et al.* 2016, 2019) by introducing variable diffusivity and moisture induced property shifts, which better reflect physical phenomena observed in aged aerospace-grade laminates. Moisture transport is modeled through Fick's law with direction-specific boundary conditions, providing an accurate representation of asymmetrical exposure.

A key novelty of the model lies in its ability to distinguish between relative stiffness degradation evaluated under current environmental conditions and total stiffness degradation, referenced to pristine properties. This dual approach enables a more nuanced understanding of performance loss across different laminate architectures and service scenarios. For validation, the model is benchmarked against experimental data for T800H/3631 laminates at room and elevated temperatures (Takeda and Ogihara 1994), demonstrating close agreement and validating the underlying assumptions across a range of crack densities and fiber orientations.

In summary, this work contributes to the advancement of composite damage modeling by addressing a significant and previously underexplored gap in the literature. It offers a practical and physically grounded analytical tool for assessing long-term laminate performance in real operational conditions, particularly where environmental gradients and multi-mode damage coexist. The outcomes not only inform more resilient composite design for aerospace and structural applications but also lay the groundwork for future studies incorporating progressive failure, aging kinetics, and advanced repair strategies.

2. Theoretical analysis

2.1 Stiffness reduction model

A symmetric [θ/90]s angle-ply laminate subjected to uniaxial loading conditions is examined. It is postulated that the 90° ply has developed continuous intralaminar cracks, and a delamination of length 2a has formed at each tip of the transverse cracks, as illustrated in Fig. 1. The spacing between the transverse cracks is denoted as $2l_0$.

The loading is applied exclusively in the x-direction, and the far-field applied stress, denoted as σ_c, is defined by the relationship $\sigma_c = \left(\frac{1}{2}h\right)N_x$, where N_x represents the applied load. The

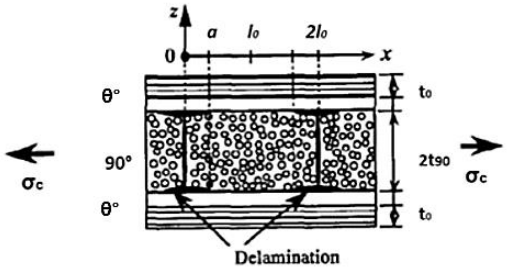

Fig. 1 Composite laminates with transverse cracks and delamination

subsequent analysis will be conducted under the assumption of a generalized plane strain condition.

$$\varepsilon_y^{\theta} = \varepsilon_y^{90} = \varepsilon_y = const \tag{1}$$

The symbol ($\bar{}$) over stress and strain components denotes volume average. They are calculated using the following expressions

- In the θ° layer.

$$\overline{f^{\theta}} = \frac{1}{2l_{\theta}}\frac{1}{t_{\theta}}\int_{-l_0}^{+l_0}\int_{t_{90}}^{h} f^{\theta}\,dx\,dz = \frac{1}{2\bar{l_0}}\frac{1}{\alpha}\int_{-\bar{l_0}}^{+\bar{l_0}}\int_{1}^{\bar{h}} f^{\theta}(\bar{x},\bar{z})d\bar{x}\,d\bar{z} \tag{2}$$

- In the 90° layer.

$$\overline{f^{90}} = \frac{1}{2l_0}\frac{1}{t_{90}}\int_{-l_0}^{+l_0}\int_{0}^{t_{90}} f^{90}dx\,dz = \frac{1}{2\bar{l_0}}\frac{1}{\alpha}\int_{-\bar{l_0}}^{+\bar{l_0}}\int_{0}^{1} f^{90}(\bar{x},\bar{z})d\bar{x}\,d\bar{z} \tag{3}$$

Where, l_0 denote the half spacing between the transverse cracks and α, is stacking parameter of layer θ° and 90°

By utilizing the strains in the 0° layer, which remains undamaged and thus exhibits strains equivalent to those of the laminate (i.e., $\varepsilon_x = \bar{\varepsilon}_x^0$, etc.), and under the assumption that residual stresses are negligible, the Young's modulus of the cracked laminate can be expressed by the following relationship

$$E_x = \frac{\sigma_c}{\bar{\varepsilon}_x^0} \tag{4}$$

Note that the initial laminate modulus measured at the same load is $E_{x0} = \frac{\sigma_c}{\varepsilon_{x0}}$ and, hence

$$\frac{E_x}{E_{x0}} = \frac{\varepsilon_{x0}}{\bar{\varepsilon}_x^0} \tag{5}$$

2.2 Stress and strain perturbation caused by transverse cracks

Constitutive equations that give the relationship between strain and stresses are:

- In the 90° layer.

$$\begin{Bmatrix}\varepsilon_x^{90}\\ \varepsilon_y^{90}\\ \varepsilon_z^{90}\end{Bmatrix} = \begin{bmatrix}S_{22} & S_{12} & S_{23}\\ S_{12} & S_{11} & S_{12}\\ S_{32} & S_{12} & S_{22}\end{bmatrix}\begin{Bmatrix}\sigma_x^{90}\\ \sigma_y^{90}\\ \sigma_z^{90}\end{Bmatrix} \tag{6}$$

- In the $\theta°$ layer.

$$\begin{Bmatrix} \varepsilon_x^\theta \\ \varepsilon_y^\theta \\ \varepsilon_z^\theta \end{Bmatrix} = \begin{bmatrix} S_{11} & S_{12} & S_{13} \\ S_{12} & S_{22} & S_{23} \\ S_{13} & S_{23} & S_{33} \end{bmatrix} \begin{Bmatrix} \sigma_x^\theta \\ \sigma_y^\theta \\ \sigma_z^\theta \end{Bmatrix} \tag{7}$$

Here, S_{ij} represents the compliance matrix for a unidirectional composite with a $\theta°$ fiber orientation. To determine the elastic properties of the laminate, it is necessary to evaluate $\bar{\varepsilon}_x^\theta$. By averaging Eqs. (3) and (4), the averaged constitutive equations for the 90° and $\theta°$ layers are derived. In these averaged relationships, the condition $\bar{\sigma}_z^{90} = \bar{\sigma}_z^\theta = 0$ holds, which arises from the force equilibrium in the z-direction.

$$\int_{-l_0}^{+l_0} \sigma_z^i \, dx = 0, \quad i = 90, \theta \tag{8}$$

Averaged constitutive equations corresponding to in-plane normal stress and strain components are

$$\begin{Bmatrix} \bar{\varepsilon}_x^\theta \\ \varepsilon_y \end{Bmatrix} = \begin{bmatrix} S_{11} & S_{12} \\ S_{12} & S_{22} \end{bmatrix} \begin{Bmatrix} \bar{\sigma}_x^\theta \\ \bar{\sigma}_y^\theta \end{Bmatrix} \tag{9}$$

$$\begin{Bmatrix} \bar{\varepsilon}_x^{90} \\ \varepsilon_y \end{Bmatrix} = \begin{bmatrix} S_{22} & S_{12} \\ S_{12} & S_{11} \end{bmatrix} \begin{Bmatrix} \bar{\sigma}_x^{90} \\ \bar{\sigma}_y^{90} \end{Bmatrix} \tag{10}$$

Eqs. (9) and (10) are derived from the three-dimensional strain-stress relationships, however, due to the condition imposed by Eq. (8), the results align with those obtained from (CLT). Specifically, for an undamaged laminate, the averaged stresses and strains are equivalent to the stresses and strains predicted by laminate theory. Consequently, Eqs. (9) and (10) remain valid and applicable under these conditions.

Force equilibrium equations for a damaged (or undamaged) laminate are:

- In *x*-direction:

$$N_x = \int_0^{t_{90}} \sigma_x^{90} dz + \int_{t_{90}}^{h} \sigma_x^\theta dz = \sigma_c (t_{90} + t_\theta) \tag{11}$$

Leading to $$\bar{\sigma}_x^{90} t_{90} + \bar{\sigma}_x^\theta t_0 = \sigma_c (t_{90} + t_\theta) \tag{12}$$

- In *y*-direction:

$$N_y = 0 \implies \int_0^{t_{90}} \sigma_y^{90} dz + \int_{t_{90}}^{h} \sigma_y^\theta dz = 0 \tag{13}$$

From which follows $$\bar{\sigma}_y^{90} t_{90} + \bar{\sigma}_y^\theta t_0 = 0 \tag{14}$$

Eqs. (9), (10), (12), and (14) collectively involve seven unknowns: four stress components and three strain components ($\bar{\varepsilon}_x^{90}, \bar{\varepsilon}_x^0$ and ε_y). The total number of available equations is six. As a result, one of the unknowns can be treated as an independent variable, while the remaining unknowns can be expressed as linear functions of this independent variable. By selecting the stress component $\bar{\sigma}_x^{90}$ as the independent variable and solving the system of Eqs. (9), (10), (12), and (14) with respect to it, the following expressions are obtained

$$\varepsilon_y = g_1 \bar{\sigma}_x^{90} + f_1 \sigma_c \,, \bar{\varepsilon}_x^{90} = g_2 \bar{\sigma}_x^{90} + f_2 \sigma_c \,, \bar{\varepsilon}_x^\theta = g_3 \bar{\sigma}_x^{90} + f_3 \sigma_c \tag{15}$$

Expressions for g_i, f_i, i=1,2,3 through laminate geometry and properties of constituents are given as follows

$$g_1 = t_{90}\frac{S_{12}S_{22}-S_{11}S_{12}}{S_{11}t_\theta+S_{22}t_{90}}\ , f_1 = \frac{S_{11}S_{12}(t_\theta+t_{90})}{S_{11}t_\theta+S_{22}t_{90}} \tag{16}$$

$$g_2 = S_{22} - \frac{S_{12}(S_{12}t_\theta+S_{12}t_{90})}{S_{11}t_\theta+S_{22}t_{90}}\ , f_2 = \frac{S_{12}S_{12}(t_\theta+t_{90})}{S_{11}t_\theta+S_{22}t_{90}} \tag{17}$$

$$g_3 = \frac{t_{90}}{t_\theta}\left(S_{12}\frac{(S_{12}t_\theta+S_{12}t_{90})}{S_{11}t_\theta+S_{22}t_{90}} - S_{11}\right)\ , f_3 = \frac{t_\theta+t_{90}}{t_\theta}\left(S_{11} - \frac{(S_{12})^2t_{90}}{S_{11}t_\theta+S_{22}t_{90}}\right) \tag{18}$$

To derive an expression for the average stress $\bar{\sigma}_x^{90}$ within the repeatable unit, the axial stress perturbation induced by the presence of two cracks is examined. Without loss of generality, the axial stress distribution can be expressed in the following form

$$\sigma_x^{90} = \sigma_{x0}^{90} - \sigma_{x0}^{90}f_1(\bar{x},\bar{z}) \tag{19}$$

$$\sigma_x^{\theta} = \sigma_{x0}^{\theta} + \sigma_{x0}^{90}f_2(\bar{x},\bar{z}) \tag{20}$$

Here, σ_{x0}^{90} represents the stress in the 90° layer as predicted by (CLT), and σ_{x0}^{0} denotes the (CLT) stress in the 0° layer (obtained through standard laminate theory procedures). The terms $-\sigma_{x0}^{90}f_1(\bar{x},\bar{z})$ and $\sigma_{x0}^{90}f_2(\bar{x},\bar{z})$ account for the stress perturbations caused by the presence of cracks. For convenience, normalization factors in the form of far-field stresses are incorporated into the perturbation functions. By averaging Eqs (19) and (20) and applying the integral force equilibrium condition in the x-direction (Eq. (11)), the following expressions are obtained

$$\bar{\sigma}_x^{90} = \sigma_{x0}^{90} - \sigma_{x0}^{90}\frac{1}{2\bar{l_0}}R(\bar{l_0}) \tag{21}$$

$$\bar{\sigma}_x^{0} = \sigma_{x0}^{\theta} + \sigma_{x0}^{90}\frac{1}{2\alpha\bar{l_0}}R(\bar{l_0}) \tag{22}$$

In the following function

$$R(\bar{l_0}) = \int_{-\bar{l_0}}^{+\bar{l_0}}\int_0^1 f_1(\bar{x},\bar{z})\,d\bar{z}\,d\bar{x} \tag{23}$$

The function $R(\bar{l_0})$ is referred to as the stress perturbation function. It characterizes the axial stress perturbation within the 90° layer and is dependent on the crack density.

The average stress $\bar{\sigma}_x^{90}$, which appears in Eq. (15), is now expressed in terms of the stress perturbation function (Eq. (23)). The conditions employed to derive Eq. (15) are consistent with those used in (CLT). Consequently, by substituting $\bar{\sigma}_x^{90} = \sigma_{x0}^{90}$, where σ_{x0}^{90} represents the *x*-axis stress in the 90° layer as per CLT, the CLT solution is obtained: $\bar{\varepsilon}_x^{90} = \varepsilon_{x0}^{90} = \varepsilon_{x0}$ $\bar{\varepsilon}_x^{0} = \varepsilon_{x0}^{0} = \varepsilon_{x0}$, and $\varepsilon_y = \varepsilon_{y0}$.

By substituting Eq. (21), which consists of two terms, into Eq. (15), the resulting expression also contains two terms. The first term, as discussed earlier, corresponds to the strain predicted by (CLT). However, the second term introduces a new component associated with the stress perturbation function $R(\bar{l_0})$

$$\varepsilon_y = \varepsilon_{y0} - \sigma_{x0}^{90}g_1\frac{1}{2\bar{l_0}}R(\bar{l_0}) \tag{24}$$

$$\bar{\varepsilon}_x^{90} = \varepsilon_{x0} - \sigma_{x0}^{90}g_2\frac{1}{2\bar{l_0}}R(\bar{l_0}) \tag{25}$$

$$\bar{\varepsilon}_x^{\theta} = \varepsilon_{x0} - \sigma_{x0}^{90} g_3 \frac{1}{2\bar{l}_0} R(\bar{l}_0) \tag{26}$$

The stress σ_{x0}^{90} in the 90° layer of an undamaged laminate under mechanical loading may be calculated using CLT

$$\sigma_{x0}^{90} = Q_{22}\varepsilon_{x0}(1 - \upsilon_{12}\upsilon_{xy}^{0}) \tag{27}$$

Here, υ_{xy}^{0} is the Poisson's ratio of the undamaged laminate.

υ_{12} is the Poisson's ratio of θ° layer

2.3 Stress and strain perturbation caused by transverse cracks and delamination

In the delaminate damage range, $l\text{-}a \leq x \leq l$, 90° layer cannot bear any load due to the transverse cracks, we therefore have

$$\overline{\sigma_{xx}^{\theta}} = \frac{t_\theta + t_{90}}{t_0}\,\overline{\sigma_c} \tag{28}$$

$$\overline{\sigma_{xx}^{90}} = 0 \tag{29}$$

t_θ and t_{90} are the thickness of θ°-layer and 90° layer respectively, $\overline{\sigma_c}$ is the average stress.

However, in the non-delaminated range, $0 \leq x \leq l\text{-}a$, 0° layer and 90° layer bearing the load jointly. Stress of θ° layer is determined as

$$\overline{\sigma_{xx}^{\theta}} = \overline{\sigma_c}\,\frac{E_0}{E_{x0}}\left[1 + \frac{t_{90}}{t_\theta}\frac{E_{90}}{E_\theta}\frac{\cosh(\xi\bar{l}_0\frac{x}{l_0})}{cosh(\xi\bar{l}_0)}\right] \tag{30}$$

The Stress of 90° layer is

$$\overline{\sigma_{xx}^{90}} = \overline{\sigma_c}\,\frac{E_0}{E_{x0}}\left[1 - \frac{\cosh(\xi\bar{l}_0\frac{x}{l_0})}{cosh(\xi\bar{l}_0)}\right] \tag{31}$$

Where ξ is the shear-lag parameter.

Since the longitudinal strains in the delaminated and non-delaminated regions differ, the average longitudinal strain is calculated as follows

$$\begin{aligned}\varepsilon_c \approx \bar{\varepsilon}_x^{\theta} &= \frac{1}{l_0}\int_0^{l_0}\frac{\overline{\sigma_{xx}^{\theta}}}{E_\theta}dx \\ &= \frac{1}{l_0}\int_{l_0-a}^{l_0}\frac{t_\theta + t_{90}}{E_\theta t_\theta}\sigma_c dx + \frac{1}{l_0}\int_{l_0-a}^{l_0}\frac{\sigma_c}{E_{x0}}\left(1 + \frac{t_{90}E_{90}\cosh(\xi\bar{l}_0\frac{x}{l_0})}{t_\theta E_\theta cosh(\xi\bar{l}_0)}\right)dx \\ &= \frac{a}{l_0}\frac{t_\theta + t_{90}}{E_\theta t_\theta}\sigma_c + \frac{l_0 - a}{l_0}\frac{\sigma_c}{E_{x0}} + \frac{t_{90}E_{90}}{t_\theta E_\theta E_{x0} cosh(\xi\bar{l}_0)}\frac{\sigma_c}{\xi\bar{l}_0}sinh\left(\xi\bar{l}_0(1 - \frac{a}{l_0})\right)\end{aligned} \tag{32}$$

Defining n as the delaminate propagation rate, a is half of the delaminated crack length.

2.4 Expression for elastic constant

To derive the expression for the longitudinal modulus, E_x, of the damaged laminate exhibiting only transverse cracks, the definition provided in Eq. (5) is utilized. By substituting Equation (26)

into this relationship and subsequently applying Eq. (27), the following expression is obtained

$$\frac{E_x}{E_{x0}} = \frac{1}{1+b\bar{\rho}R(\overline{l_0})} \tag{33}$$

Where $\bar{\rho} = \frac{1}{2\overline{l_0}}$, $\overline{l_0} = \frac{l_0}{t_{90}}$ is the noramalized crack density and a, b are known functions, dependent on elastic properties and geometry of the θ° and 90° layer

$$b = \frac{E_{90}t_{90}}{E_x^0 t_\theta}\left(\frac{1-\upsilon_{12}\upsilon_{xy}^0}{1-\upsilon_{12}\upsilon_{21}}\right)\left(1+\upsilon_{xy}^0\frac{S_{12}t_{90}+S_{12}t_\theta}{S_{22}t_\theta+S_{11}t_\theta}\right) \tag{34}$$

E_x^0 and E_{90} are the Young's moduli of θ° and 90° layers respectively.

From Eqs. (30) and (32), along with the relationship $\sigma_c = E_x\varepsilon_c$, and using the definitions $a = nl_0$ and $l_0 = \frac{1}{2\rho}$, the longitudinal modulus E_x of the damaged laminate, accounting for both transverse cracks and delamination, can be derived as follows:

$$\frac{E_x}{E_{x0}} = \frac{1}{E_{x0}\left(n\frac{t_\theta+t_{90}}{E_\theta t_\theta}+\frac{1-n}{E_{x0}}+\frac{t_{90}E_{90}\left[\frac{2\rho}{n\xi}sinh\left(\frac{(1-n)\xi}{2\rho}\right)\right]}{t_\theta E_\theta E_{x0}cosh(\frac{n\xi}{2\rho})}\right)} \tag{35}$$

From Eqs. (33) and (35), it is evident that the functions $R(\overline{l_0})$ and ξ are the only unknowns. Consequently, the reduction in the Young's modulus is dependent on the form of these functions as they relate to crack density. Solutions for these functions can be determined using various analytical models, such as shear-lag models.

2.5 Computation of the stress perturbation function using shear lag model

In this study, two models developed by Berthelot *et al.* (1996) are employed. These models have been modified by incorporating the stress perturbation function. The stress perturbation function $R(\overline{l_0})$ is determined as follows

$$R(a) = \int_{-\overline{l_0}}^{+\overline{l_0}} \frac{\cosh(\xi\bar{x})}{\cosh(\xi\overline{l_0})}d\bar{x} = \frac{2}{\xi}\tanh(\xi\overline{l_0}) \tag{36}$$

Where

$$\xi^2 = \bar{G}\frac{t_{90}(t_{90}E_{90}+t_\theta E_\theta)}{t_\theta E_{90}E_\theta} \tag{37}$$

The coefficient $\overline{G}$ depends on used assumptions about the longitudinal displacement and shears stress distribution:

• The first case assumes that the longitudinal displacement follows a parabolic distribution through the thickness of the 90° layer

$$u_{90}(x,z) = \overline{u_{90}}(x) + \left(z^2 - \frac{t_{90}^2}{3}\right)A_{90}(x) \tag{38}$$

The variation of the longitudinal displacement is determined through the thickness of the θ° layers.

$$u_\theta(x,z) = \overline{u_\theta}(x) + f(z)A_\theta(x) \tag{39}$$

• The second case assumes that the shear stresses, which are similar in both the θ° and 90°

layers, can be derived by considering the transverse displacement to be independent of the longitudinal coordinate

$$\sigma_{xz}^{i} = G_{xz}^{i}\,\gamma_{xz}^{i} \tag{40}$$

$$\gamma_{xz}^{i} = \frac{\partial u_i}{\partial z} + \frac{\partial w_i}{\partial x} \approx \frac{\partial u_i}{\partial z} \qquad i = \theta°, 90° \tag{41}$$

The coefficient $\overline{G}$ is done by

$$\bar{G} = \frac{3G}{t_{90}} \tag{42}$$

The shear modulus *G* of the elementary cell

$$G = \frac{G_{xz}^{90}}{1-3\frac{G_{xz}^{90}}{G_{xz}^{\theta}}\frac{f(t_{90})}{t_{90}f'(t_{90})}} \tag{43}$$

Two distinct analytical functions describing the variation have been considered, as proposed by Berthelot *et al.* (1996):

• In the case where a parabolic variation of longitudinal displacement is assumed in both the $\theta°$ and 90° layers

By replacing the function $f(z) = z^2 - 2(t_\theta + t_{90})z + \frac{2}{3}t_\theta^2 + 2t_\theta t_{90} + t_{90}^2$ in the Eq. (43), the shear modulus for parabolic assumption will be in the form

$$G = \frac{G_{xz}^{90}}{1+\alpha\frac{G_{xz}^{90}}{G_{xz}^{\theta}}} \tag{44}$$

• In the case where the variation of the longitudinal displacement is assumed to be progressive within the $\theta°$ layer:

We use the function $f(z) = \frac{sinh\alpha\eta_t}{\alpha\eta_t} - cosh\ \eta_t(1 + \alpha - \frac{z}{t_{90}})$ in the Eq. (43), the shear modulus for progressive shear assumption will be in the form

$$G = \frac{G_{xz}^{90}}{1+3\alpha\frac{\alpha\eta_t(tanh\alpha\eta_t)^{-1}-1}{\alpha\eta_t{}^2}\frac{G_{xz}^{90}}{G_{xz}^{\theta}}} \tag{45}$$

η_t is the shear transfer parameter.

3. Results and discussion

A computational algorithm, based on the aforementioned equations, was developed to calculate the reduction in stiffness for angle-ply laminates resulting from transverse ply cracking and delamination.

3.1 Validation of the predicted model

In this section, the results of the current program will be validated without accounting for the hygrothermal effects on the material properties. The predictions will be compared with experimental data obtained for T800H/3631 laminates, whose elastic properties are provided in

Table 1 Material properties of T800H/3631 laminate used in calculations (Takeda and Ogihara 1994)

T800H/3631	Room temperature (RT)	80°C
E_0 (GPa)	152.2	144.2
E_{90} (GPa)	9.57	8.09
G_0 (GPa)	4.5	4.26
G_{90} (GPa)	3.21	2.75
v_0	0.349	0.349
v_{90}	0.490	0.490

Table 2 Comparison of experimental and analytical models for stiffness degradation in T800H/3631 laminate at room temperature

Crack density	Experimental	At room temperature (RT)			
		Parabolic analysis	Error (%)	Progressive shear	Error (%)
0.25	0.9803	0.9714	0.89%	0.9717	0.85%
0.50	0.9742	0.9573	1.69%	0.9602	1.39%
0.75	0.9542	0.9453	0.89%	0.9489	0.53%
0.95	0.9509	0.9362	1.48%	0.9388	1.21%
1.00	0.9401	0.9319	0.82%	0.9345	0.56%
1.10	0.9284	0.9286	0.02%	0.9312	0.29%
1.30	0.9087	0.9216	1.29%	0.9232	1.46%

Table 3 Comparison of experimental and analytical models for stiffness degradation in T800H/3631 laminate under elevated temperature (80°C) conditions

Crack density	Experimental	At 80 °C			
		Parabolic analysis	Error (%)	Progressive shear	Error (%)
0.10	0.9893	0.9875	0.18%	0.9882	0.11%
0.15	0.9836	0.9856	0.20%	0.9864	0.28%
0.45	0.9804	0.9691	1.13%	0.9722	0.82%
0.55	0.9649	0.9638	0.11%	0.9672	0.23%
0.65	0.9591	0.9577	0.14%	0.9611	0.20%

Table 1 (Takeda and Ogihara 1994). Each ply has a thickness of approximately 0.132 mm, and the fiber volume fraction is approximately 0.6.

The analytical models for stiffness degradation in T800H/3631 laminate align closely with experimental trends from Takeda and Ogihara (1994), validating their applicability at room temperature (Table 2). Model discrepancies at elevated crack densities suggest limitations in capturing nonlinear damage accumulation or microcrack interactions. The progressive shear framework shows marginally enhanced fidelity, likely due to its refined treatment of shear-driven damage mechanisms.

Under thermal exposure, both models demonstrate robust agreement with experimental stiffness loss data, emphasizing their utility for T800H/3631 laminates in thermally stressed environments (Table 3). Minor asymmetrical errors imply temperature-dependent shifts in matrix-dominated degradation processes. These results corroborate the foundational experimental work of Takeda and Ogihara, while underscoring the need for thermal-kinetic refinements in predictive

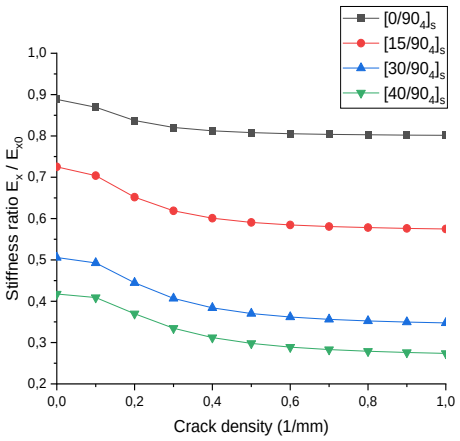

Fig. 2 Young's modulus reduction as function of crack density for T800H/3631 [θ/90$_4$]$_s$ laminate at room temperature

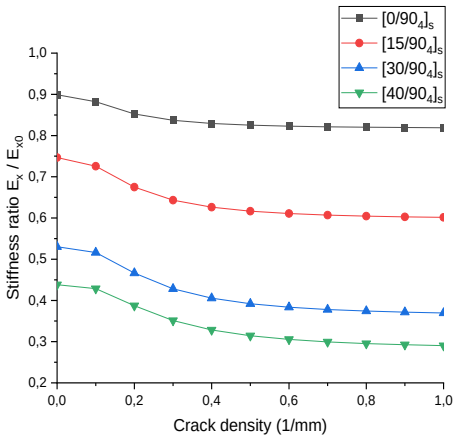

Fig. 3 Young's modulus reduction as function of crack density for T800H/3631 [θ/90$_4$]$_s$ laminate at 80°C

frameworks. The progressive shear model closely matches the experimental stiffness degradation at low crack densities, reflecting gradual damage accumulation. In contrast, the parabolic model shows better agreement with experiments at higher crack densities, where stiffness drops more sharply. This trade-off justifies using each model based on the damage level despite computational differences.

The Figs. 2 and 3 show a nonlinear decrease in Young's modulus as crack density increases, following a parabolic trend. At low crack densities, stiffness reduction is gradual, but it accelerates as cracks propagate and interact. Higher fiber angles (θ) lead to greater stiffness loss due to weaker load-bearing capacity in the primary direction. Temperature (80°C) exacerbates modulus degradation, indicating increased matrix softening and damage propagation. Overall, fiber orientation and temperature significantly influence the laminate's stiffness degradation behavior.

3.2 Influence of asymmetrical environmental conditions on stiffness degradation

This study investigates the reduction in stiffness caused by transverse cracking and delamination in an angle ply composite laminate under asymmetrical environmental conditions. The distribution model of Sereir *et al.* (2006) is used based on the Tsai model (1988) to incorporate aging effects and observe their progression at both the fiber and matrix scales. The methodology of this simplified approach involves accounting for the actual distribution of moisture concentration within each ply by employing its series expansion (Vergnaud 1992). This enables the accurate determination of stiffness under the influence of hygrothermal effects.

Tsai (1988) introduces a dimensionless temperature parameter, T^*, which serves as the critical variable for evaluating the influence of hygrothermal conditions on stress distribution

$$T^* = \frac{T_g - T_{opr}}{T_g - T_{rm}} \tag{46}$$

Here, T_g represents the glass transition temperature, T_{opr} denotes the operating temperature, and T_{rm} is the room temperature. Furthermore, it is assumed that moisture reduces the glass transition

Table 4 Fiber and matrix characteristics of graphite/epoxy material (T300/5208) (Tsai 1988) (T=22℃ and C=0.5%)

E_{fx}^0 (Gpa)	E_{fx}^0 (Gpa)	E_m^0 (Gpa)	ν_{fx}^0	ν_m^0	G_{fx}^0 (Gpa)	G_m^0 (Gpa)	V_f
259	18.69	3.4	0.25	0.35	19.69	1.26	0.7

Table 5 Parameters of temperature and moisture characteristics variation (Tsai 1988)

T_g^0 (℃)	T_{room} (℃)	g (℃/c)	d	f
160	22	2000	0.35	0.04

temperature T_g^0 through a straightforward temperature shift.

$$T_g = T_g^0 - g \cdot c \tag{47}$$

Here, T_g^0 represents the glass transition temperature in the dry state, g denotes the temperature shift per unit of absorbed moisture, and c is the absorbed moisture content. The exponents of T^* can be employed to empirically model the mechanical properties of the matrix as a function of both moisture and temperature.

$$\frac{E_m}{E_m^0} = \frac{G_m}{G_m^0} = \frac{\nu_m}{\nu_m^0} = (T^*)^d \tag{48}$$

E_m^0, $G_m^0$and ν_m^0 are the Young's modulus, shear modulus and Poisson's ratio, respectively, of the matrix at room temperature and d is an empirical constant. The same exponents of T^* is used to empirically fit the fiber mechanical properties as function of moisture and temperature.

$$\frac{E_{fx}}{E_{fx}^0} = \frac{E_{fy}}{E_{fy}^0} = \frac{G_{fx}}{G_{fx}^0} = \frac{\nu_{fx}}{\nu_{fx}^0} = (T^*)^f \tag{49}$$

E_{fx}^0, E_{fy}^0, G_{fx}^0 and ν_{fx}^0 are the longitudinal and transversal Young's modulus, shear modulus and Poisson's ratio, respectively, of the fiber at room temperature and f is an empirical constant.

It is assumed that E_m, G_m,ν_m, E_{fx}, E_{fy}, G_{fx} and ν_{fx} are function of temperature and moisture (as Eqs. (48) and (49)), then E_x, E_y and G_{xy} will be also function of temperature and moisture.

A material is mainly characterized by its mechanical moduli, which can be determined experimentally. For example, several tensile tests are required to determine the elastic properties of a unidirectional fiber-reinforced composite. The longitudinal Young's modulus and Poisson's ratio are measured using a 0° unidirectional tensile test, while the transverse modulus is measured with a 90° test, and the shear modulus with a 45° test. To characterize the material, we select appropriate models for each modulus. The longitudinal Young's modulus and Poisson's ratio are based on the rule of mixtures, while the transverse modulus and Poisson's ratio follow Hahn's modified rule, also used in studies by Sereir *et al.* (2006). In Tables 4 and 5, we identified the parameters that influence the mechanical characteristics of graphite/epoxy material.

Let's consider a laminated plate of thickness h made of polymer matrix composite, with both sides subjected to different dry environments. The plate is assumed to be infinite in both x and y directions, with moisture variation occurring only in the z direction (refer to Fig. 4). Consequently, the problem is one-dimensional. The lower side of the plate has a moisture concentration C_1 and a temperature T, the upper side has a concentration C_2 and a temperature T, the moisture concentration within the plate is governed by the Fick equation (Shen and Springer 1981,

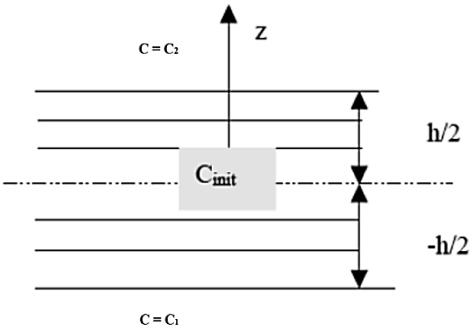

Fig. 4 Moisture diffusion effect

Table 4 Moisture diffusion characteristics (Sereir *et al.* 2006)

Diffusivity, mm^2/s	$D_z = 132\exp(-6750/T)$ T: Temperature (K)
Moisture concentration at the surface as a function of relative humidity, %	$C_1 = 0.015 \cdot HR_1, HR_1 = 100\%$ $C_2 = 0.015 \cdot HR_2, HR_1 = 50\%$ H: Relative humidity (%)

Benkhedda *et al.* 2008) with a diffusivity D_z.

$$\frac{\partial C}{\partial t} = D_z \frac{\partial^2 C}{\partial z^2} \tag{50}$$

C_1 and C_2 refer to surface concentrations on the bottom and top laminate faces, respectively.
With

$$C=C(z,t) \text{ at } t=0 \text{ for } 0 < z < h \tag{51}$$

$$\begin{aligned} C&=C_2 \text{ at } t>0 \text{ for } z = h \\ C&=C_1 \text{ at } t>0 \text{ for } z = 0 \end{aligned} \tag{52}$$

The moisture diffusion characteristics are given in Table 4.
The initial conditions being uniform and the boundary conditions are constants, the unidimensional solution of Fick equation can be expressed as (Sereir *et al.* 2006)

$$C(z_k,t) = \left[C_1 + (C_2 - C_1)\frac{z_k}{h} + \frac{2}{\pi}\sum_{n=1}^{\infty} \frac{C2\cos(n\pi) - C1}{n} \times \sin\left(\frac{n\pi z_k}{h}\right) \exp\left(\frac{-D_z n^2 \pi^2 t}{h^2}\right)\right] \tag{53}$$

Very often, the laminated composite plate is symmetrical about the central plane (Fig. 4), and for the concentration's formulations are the most convenient if we take the surfaces at $z = \pm h/2$.
When z_k is replaced by $z_k \pm h/2$

$$\begin{aligned} C&=C_2 \text{ at } t>0 \text{ for } z = +\frac{h}{2} \\ C&=C_1 \text{ at } t>0 \text{ for } z = -\frac{h}{2} \end{aligned} \tag{54}$$

3.2.1 Relative stiffness degradation

Time t being given, the first step is to compute the on-axis free expansions E_x, E_y, G_{xy} and υ_{xy}.

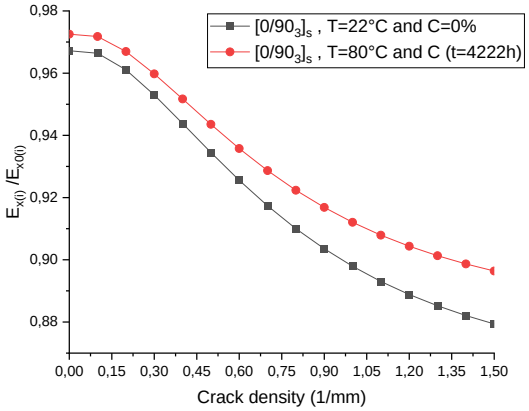

Fig. 5 Relative stiffness degradation as function of crack density for [0/90$_3$]$_s$ laminate under different hygrothermal conditions

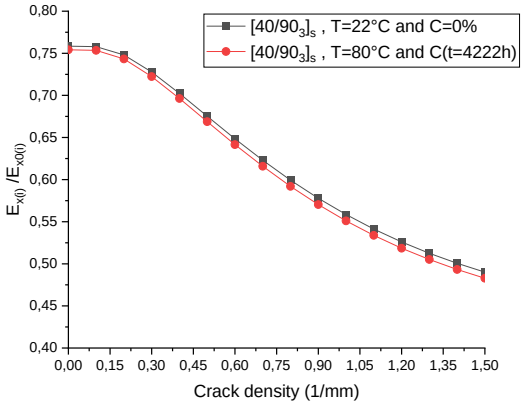

Fig. 6 Relative stiffness degradation as function of crack density for [40/90$_3$]$_s$ laminate under different hygrothermal conditions

These expansions are computed at each point z_k of thickness. Finally, the relative stiffness degradation in the angle ply [θ/90$_3$]$_s$ composite laminate due to crack density with transverse cracks and delamination is evaluated, compared to the initial stiffness of the same uncracked laminate under the same environmental conditions. It should be noted that this initial stiffness of the uncracked laminate is a function of temperature and moisture distribution. Consequently, Eq. (35) become

$$\frac{E_{x(i)}}{E_{x0(i)}} = \frac{1}{E_{x0(i)}\left(n\frac{t_\theta + t_{90}}{E_{\theta(i)} t_\theta} + \frac{1-n}{E_{x0(i)}} + \frac{t_{90} E_{90(i)} \left[\frac{2\rho}{n\xi_{(i)}} sinh\left(\frac{(1-n)\xi_{(i)}}{2\rho} \right) \right]}{t_\theta E_{\theta(i)} E_{x0(i)} cosh\left(\frac{n\xi_{(i)}}{2\rho} \right)} \right)} \tag{55}$$

The index (i) represents the considered case of environmental conditions.

a) Hygrothermal effect on the relative stiffness degradation

The relative stiffness degradation in [θ/90$_3$]s composite laminates increases nonlinearly with crack density, with a sharper drop at higher densities due to transverse cracks and delamination (Figs. 5 and 6). [40/90$_3$]s laminates exhibit greater stiffness loss than [0/90$_3$]$_s$, as higher fiber angles reduce axial load transfer efficiency, amplifying interlaminar shear stresses and delamination. Hygrothermal effects (80°C, high humidity) accelerate matrix softening, weakening fiber-matrix adhesion and increasing damage propagation. Transverse cracks act as stress concentrators, leading to progressive stiffness degradation, while delamination separates load-bearing layers, further reducing structural integrity. These results highlight the importance of fiber orientation and environmental conditions in composite durability, reinforcing the need for optimized laminate design for long-term performance.

b) Fiber orientation effect on the relative stiffness degradation

Table 6 illustrates the relative stiffness degradation as a function of crack density for different fiber orientations, under two environmental conditions (22°C, 0% humidity and 80°C and C(t=100h)). The results show a nonlinear increase in stiffness degradation with crack density,

Table 6 Relative stiffness degradation as function of crack density and different fiber orientation angle and hygrothermal conditions

Relative stiffness degradation	Laminate	Crack density	T=22°C and C=0%				T=80°C and C(t=100h)			
			θ=0°	θ=15°	θ=30°	θ=40°	θ=0°	θ=15°	θ=30°	θ=40°
	$[\theta°/90°]_s$	0	1.12%	2.75%	6.67%	9.59%	0.94%	2.67%	6.79%	9.80%
		0,5	1.33%	3.04%	7.26%	10.32%	1.12%	2.97%	7.41%	10.55%
		1	1.94%	4.09%	9.47%	13.15%	1.65%	4.02%	9.69%	13.46%
		1,5	2.60%	5.34%	12.09%	16.52%	2.22%	5.27%	12.37%	16.91%
	$[\theta°/90_3°]_s$	0	3.28%	7.82%	17.66%	24.15%	2.75%	7.61%	17.95%	24.59%
		0,5	6.55%	13.41%	25.75%	32.48%	5.65%	13.26%	26.28%	33.12%
		1	10.21%	20.41%	36.51%	44.15%	8.80%	20.18%	37.17%	44.90%
		1,5	12.06%	24.29%	42.67%	50.99%	10.36%	23.94%	43.31%	51.72%
	$[\theta°_3/90°]_s$	0	0.38%	0.93%	2.33%	3.42%	0.31%	0.91%	2.37%	3.50%
		0,5	0.38%	0.94%	2.33%	3.43%	0.32%	0.91%	2.38%	3.51%
		1	0.43%	0.97%	2.44%	3.59%	0.36%	0.95%	2.49%	3.67%
		1,5	0.51%	1.06%	2.68%	3.95%	0.43%	1.03%	2.74%	4.04%

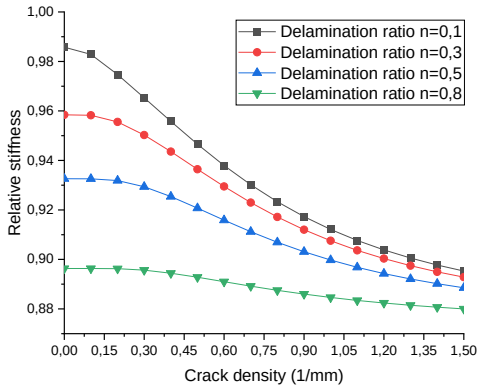

Fig. 7 Relative stiffness degradation as function of crack density for $[0/90_3]_s$ laminate at 80°C and C(t=100h)

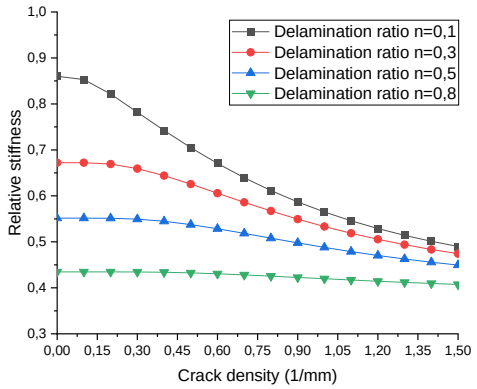

Fig. 8 Relative stiffness degradation as function of crack density for $[40/90_3]_s$ laminate at 80°C and C(t=100h)

where higher fiber angles (θ=40°) lead to greater stiffness loss due to reduced axial load transfer and increased interlaminar shear stress. Hygrothermal aging at 80°C exacerbates stiffness degradation, with moisture absorption softening the matrix and weakening fiber-matrix adhesion, accelerating damage propagation. The $[40/90_3]_s$ laminate exhibits the most severe degradation (~51.72% at 80°C, crack density 1.5) due to increased delamination susceptibility, while $[0/90_3]$s laminates maintain better load-bearing capacity. The $[\theta/90_3]_s$ configuration shows greater vulnerability than $[\theta_3/90°]_s$ due to thinner $\theta°$ layers, which offer less resistance to delamination. These results confirm that fiber orientation and environmental conditions critically influence composite durability, emphasizing the need for optimized laminate design in harsh conditions.

c. Delamination ratio effect on the relative stiffness degradation

Figs. 7 and 8 illustrate stiffness degradation in $[0/90_3]$s and $[40/90_3]$s laminates at 80°C and

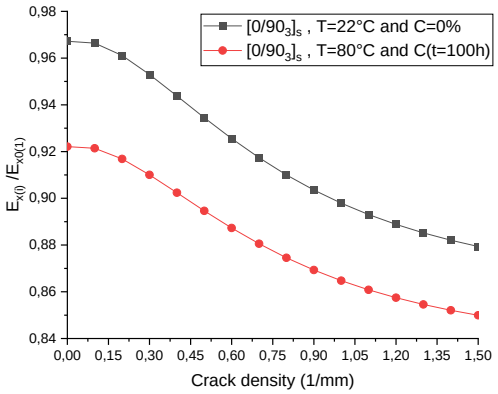

Fig. 9 Total stiffness degradation as function of crack density for $[0/90_3]_s$ laminate under different hygrothermal conditions

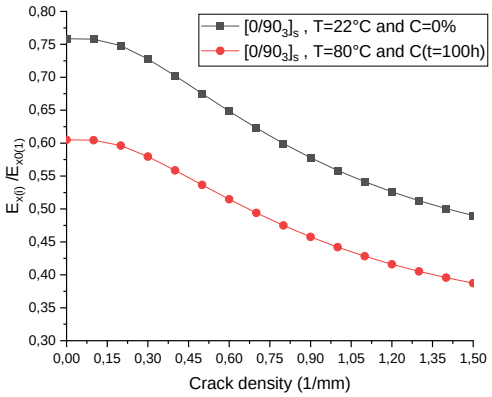

Fig. 10 Total stiffness degradation as function of crack density for $[40/90_3]_s$ laminate under different hygrothermal conditions

1.5% humidity with different delamination ratio. The $[40/90_3]$s laminate (Fig. 8) exhibits significantly higher degradation (e.g., ~50% vs. ~30% at high crack densities) compared to $[0/90_3]$s (Fig. 7). This disparity arises because 40° fiber orientation amplifies interlaminar shear stresses, reducing load transfer efficiency between plies. Hygrothermal aging softens the matrix and weakens fiber-matrix adhesion, accelerating delamination and crack propagation. Delamination further disrupts stress distribution, particularly in angled laminates, leading to severe stiffness loss. These results emphasize the critical role of fiber orientation in environmental durability and damage tolerance.

3.2.2 Total stiffness degradation

In this section, the total reduction in stiffness modulus is evaluated relative to the axial modulus of the uncracked laminate under the initial exposure to environmental conditions specified in standard condition (T=22°C and C=0%). As a result, this total stiffness reduction incorporates the effects of crack density, moisture, and temperature variations. Eq. (35) is modified as follows

$$\frac{E_{x(i)}}{E_{x0(1)}} = \frac{\left(t_\theta E_{\theta(i)} + t_{90} E_{90(i)}\right)}{E_{x0(i)}\left(n\frac{t_\theta + t_{90}}{E_{\theta(i)} t_\theta} + \frac{1-n}{E_{x0(i)}} + \frac{t_{90} E_{90(i)}\left[\frac{2\rho}{n\xi_{(i)}} sinh\left(\frac{(1-n)\xi_{(i)}}{2\rho}\right)\right]}{t_\theta E_{\theta(i)} E_{x0(i)} cosh\left(\frac{n\xi_{(i)}}{2\rho}\right)}\right)\left(t_\theta E_{\theta(1)} + t_{90} E_{90(1)}\right)} \tag{55}$$

a) Hygrothermal effect on the total stiffness degradation

Figs. 9 and 10 illustrate total stiffness degradation for $[0/90_3]$s and $[40/90_3]$s laminates under different hygrothermal conditions, showing a more pronounced reduction compared to Figs. 5 and 6, which focused on relative stiffness. The $[40/90_3]$s laminate experiences the highest degradation (~60% at crack density 1.5) due to increased interlaminar shear stress and reduced load transfer efficiency at higher fiber angles. The presence of moisture and elevated temperature (80°C) weakens fiber-matrix adhesion, accelerating stiffness loss and delamination propagation. Unlike relative stiffness, total stiffness is more affected by hygrothermal exposure, indicating that the combined effect of transverse cracks and delamination amplifies mechanical degradation.

Table 7 Total stiffness degradation as function of crack density and different fiber orientation angle and hygrothermal conditions

Total stiffness degradation	Laminate	Crack density	*T*=22°C and *C*=0%				*T*=80°C and C(*t*=100h)			
			θ=0°	θ=15°	θ=30°	θ=40°	θ=0°	θ=15°	θ=30°	θ=40°
	$[\theta°/90°]_s$	0	1.12%	2.75%	6.67%	9.59%	4.52%	19.15%	25.23%	27.71%
		0,5	1.33%	3.04%	7.26%	10.32%	4.71%	19.40%	25.72%	28.32%
		1	1.94%	4.09%	9.47%	13.15%	5.22%	20.27%	27.55%	30.65%
		1,5	2.60%	5.34%	12.09%	16.52%	5.76%	21.30%	29.70%	33.41%
	$[\theta°/90_3°]_s$	0	3.28%	7.82%	17.66%	24.15%	7.79%	23.64%	34.19%	39.49%
		0,5	6.55%	13.41%	25.75%	32.48%	10.54%	28.31%	40.87%	46.34%
		1	10.21%	20.41%	36.51%	44.15%	13.52%	34.03%	49.60%	55.79%
		1,5	12.06%	24.29%	42.67%	50.99%	15.01%	37.13%	54.53%	61.26%
	$[\theta°_3/90°]_s$	0	0.38%	0.93%	2.33%	3.42%	3.44%	17.49%	22.33%	23.42%
		0,5	0.38%	0.94%	2.33%	3.43%	3.44%	17.50%	22.33%	23.43%
		1	0.43%	0.97%	2.44%	3.59%	3.48%	17.53%	22.42%	23.56%
		1,5	0.51%	1.06%	2.68%	3.95%	3.55%	17.60%	22.61%	23.85%

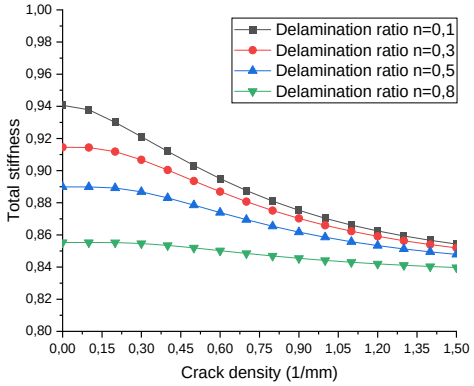

Fig. 11 Total stiffness degradation as function of crack density for $[0/90_3]$s laminate at 80°C and *C*=0%

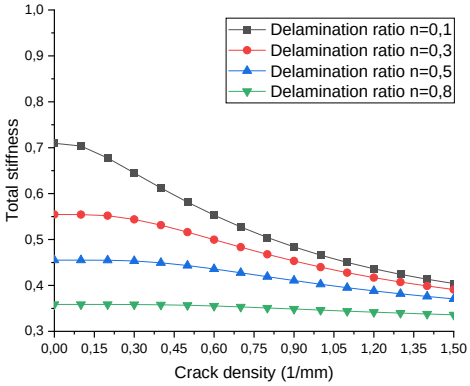

Fig. 12 Total stiffness degradation as function of crack density for $[40/90_3]$s laminate at 80°C and *C*(*t*=100h)

b) Fiber orientation effect on the total stiffness degradation

Table 7, like Table 6, shows a nonlinear increase in stiffness degradation with crack density, fiber orientation, and hygrothermal conditions. However, total stiffness is more influenced by these factors than relative stiffness, particularly at higher fiber angles (θ=40°), increased temperatures (80°C), and humidity. Additionally, in asymmetrical environmental conditions, fiber orientation plays a significant role in enhancing diffusivity, facilitating moisture absorption and accelerating matrix degradation. The most severe degradation (~61.26% at crack density 1.5 vs. 51.72% for relative stiffness) is observed in $[\theta/90_3]_s$ laminates, where interlaminar shear stress intensifies, reducing load transfer. Transverse cracks and delamination amplify stress concentrations, making the laminate more vulnerable to hygrothermal aging, as moisture absorption weakens fiber-matrix adhesion and high temperatures soften the matrix, accelerating damage propagation. In contrast, uncracked laminates retain their structural integrity longer,

exhibiting lower stiffness degradation under the same conditions.

c) Delamination ratio effect on the total stiffness degradation

Figs. 11 and 12 depict total stiffness degradation in $[0/90_3]$s and $[40/90_3]$s laminates under hygrothermal conditions and varying delamination ratios, showing a more pronounced reduction compared to Figs. 7 and 8. The $[40/90_3]$s laminate experiences the most severe stiffness loss, emphasizing the influence of interlaminar shear stress and diminished load transfer at higher fiber angles. Moisture absorption and elevated temperature (80°C) further degrade the matrix, accelerating delamination growth and stiffness reduction. The more substantial decline in total stiffness relative to relative stiffness highlights the critical role of delamination in intensifying composite deterioration. Moreover, in asymmetrical environmental conditions, delamination accelerates diffusivity, facilitating moisture penetration and amplifying material degradation, making cracked laminates significantly more vulnerable than uncracked ones.

4. Conclusions

This study presents a detailed investigation of stiffness degradation in composite laminates subjected to transverse cracks and delamination under asymmetrical environmental conditions. By integrating a modified shear-lag model with parabolic and progressive shear analysis, this research provides a more accurate prediction of stiffness reduction, differentiating it from previous studies that focused solely on transverse cracking. The originality of this work lies in the comprehensive evaluation of both relative and total stiffness, considering the combined effects of fiber orientation, delamination, and environmental exposure.

The results demonstrate that stiffness degradation increases nonlinearly with crack density, with higher fiber angles (θ=40°) experiencing the most significant reduction due to amplified interlaminar shear stress and reduced load transfer efficiency. Hygrothermal aging, exacerbates stiffness loss by softening the matrix and weakening fiber-matrix adhesion, thereby accelerating damage propagation. A key finding is that total stiffness degradation is more pronounced than relative stiffness degradation, highlighting the critical role of delamination in composite failure. The results confirm that delamination not only weakens mechanical integrity but also enhances diffusivity in asymmetrical environmental conditions, leading to faster material deterioration compared to uncracked laminates.

This research contributes to a deeper understanding of composite damage mechanisms and provides valuable insights for optimizing laminate design in aerospace, automotive, and marine applications. Unlike previous works, which mainly addressed single damage modes, this study underscores the interplay between multiple degradation factors and their combined impact on structural performance. Future studies should explore advanced mitigation strategies, such as nano-reinforced polymer matrices or self-healing composites, to enhance damage resistance and extend the lifespan of composite structures under extreme environmental conditions

References

Behera, A., Bhoi, N.K., Thawre, M.M., Ballal, A. and Das, D. (2023), "Quantification of hygrothermal aging-induced interfacial debonding of carbon fiber/epoxy composites at nano-to-micrometer length

scales", *J. Compos. Mater*., **57**(30), 4637-4647. https://doi.org/10.1177/00219983231213912.
Behera, A., Vishwakarma, A., Thawre, M.M. and Ballal, A. (2020), "Effect of hygrothermal aging on static behavior of quasi-isotropic CFRP composite laminate", *Compos. Commun*., **17**, 51-55. https://doi.org/10.1016/j.coco.2019.11.009.
Benkhedda, A., Tounsi A. and Adda Bedia, E.A. (2008), "Effect of temperature and humidity on transient hygrothermal stress during moisture desorption in laminated composite plates", *Compos. Struct.*, **82**(4), 629-635. https://doi.org/10.1016/j.compstruct.2007.04.013.
Berthelot, J.M., Leblond, P., El Mahi, A. and Le Corre, J.F. (1996), "Transverse cracking of cross ply laminates: Part I. Analysis", *Compos. Part A: Appl. Sci. Manuf*., **27**(10), 989-1001. https://doi.org/10.1016/1359-835X(96)80002-A.
Carrera, E., Cinefra, M., Petrolo, M. and Zappino, E. (2011), *Finite Element Analysis of Structures through Unified Formulation*, John Wiley & Sons.
Cheng, W. and Cao, Y. (2023), "Investigation of the hygrothermal aging behavior of GFRP laminates used for a marine unmanned aerial vehicle structure", *AIP Adv*., **13**(04), 1-16. https://doi.org/10.1063/5.0140558.
Fernandes, O., Dutta, J. and Pai, Y. (2023), "Effect of various factors and hygrothermal ageing environment on the low velocity impact response of fibre reinforced polymer composites- a comprehensive review", *J. Cogent Eng*., **10**(1), 2247228. https://doi.org/10.1080/23311916.2023.2247228.
JiYe, J., Wu, Y.S., Gao, Y., Gong, C.X., Wang, H., Xu, X.P. and Peng, H.X. (2023), "Hygrothermal aging effects on fiber-metal-laminates with engineered interfaces", *J. Compos. Commun.*, **43**, 101721. https://doi.org/10.1016/j.coco.202²3.101721.
Kesba, M.K., Benkhedda, A. and Boukert, B. (2019), "Hygrothermal effect on the moisture absorption in composite laminates with transverse cracks and delamination", *Adv. Aircraft Spacecraft Sci*., **6**(4), 315-331. https://doi.org/10.12989/aas.2019.6.4.315.
Khodjet-Kesba, M., AddaBedia, E.A., Benkhedda, A. and Boukert, B. (2016), "Prediction of Poisson's ratio degradation in hygrothermal aged and cracked $[\theta_m/90_n]_s$ composite laminates", *Steel Compos. Struct.*, **21**(1)**,** 57-72. https://doi.org/10.12989/scs.2016.21.1.057.
Khodjet-Kesba, M., Benkhedda, A., Bedia, E.A. and Boukert, B. (2018), "On transverse matrix cracking in composite laminates loaded in flexure under transient hygrothermal conditions", *Struct. Eng. Mech*., **67**(2), 165-173. https://doi.org/10.12989/sem.2018.67.2.165.
Li, W., Zhang, J., Qiao, P. and Wang, T. (2016), "Extended layerwise method for laminated composite plates with multiple delaminations and transverse cracks", *Comput. Mech.*, **58**, 657-679. https://doi.org/10.1007/s00466-016-1310-2.
Liu, Z. and Li, P. (2025), "Effect of fiber orientation of adjacent plies on the mode I delamination fracture of carbon fiber reinforced polymer multidirectional laminates", *Polym. Compos.*, **46**(3), 2560-2572. https://doi.org/10.1002/pc.29124.
Lu, Y., Wen, H., Ye, L. and Wu, D. (2018), "An extended layerwise/solid-element method of stiffened composite plates with delaminations and transverse crack", *Int. J. Mech. Mater. Des.*, **14**, 345-358. https://doi.org/10.1007/s10999-017-9378-1.
Reddy, J.N. (2004), *Mechanics of Laminated Composite Plates and Shells: Theory and Analysis*, CRC Press.
Sereir, Z., Adda-Bedia, E.A. and Tounsi, A. (2006), "Effect of temperature on the hygrothermal behaviour of unidirectional laminated plates with asymmetrical environmental conditions", *Compos. Struct*., **72**, 383-392. https://doi.org/10.1016/j.compstruct.2005.01.008.
Shen, C.H. and Springer, G.S. (1976), "Moisture absorption and desorption of composite materials", *J. Compos. Mater.*, **10**(1), 2-20. https://doi.org/10.1177/002199837601000101.
Takeda, N. and Ogihara, S. (1994), "Initiation and growth of delamination from the tips of transverse cracks in CFRP cross-ply lamainates", *Compos. Sci. Tech*., **52**, 309-318. https://doi.org/10.1016/0266-3538(94)90166-X.
Tsai, S.W. (1988), *Composites Design*, Think Composites, Dayton, Paris, Tokyo.
Varun, J.P., Mondal, P. and Mahato, P.K. (2022), "Enhancement of aeroelastic performance of a smart delaminated composite plate under hygrothermal environment", *Compos. Struct.*, **292**, 115662.

https://doi.org/10.1016/j.compstruct.2022.115662.

Vergnaud, J.M. (1992), *Drying of Polymeric and Solid Materials: Modelling and Industrial Applications*, Springer-Verlag, London.

Wang, S., Akbolat, M.Ç., Katnam, K.B., Zou, Z., Potluri, P., Sprenger, S. and Taylor, J. (2023), "The effect of hygrothermal ageing on the delamination of Carbon/epoxy laminates with Core-shell rubber nanoparticle and Micro-fibre thermoplastic veil toughening", *Compos. Part A: Appl. Sci. Manuf.*, **171**, 107576. https://doi.org/10.1016/j.compositesa.2023.107576.

Zhang, H., Song, Z., Zhang, L., Liu, Z. and Zhu, P. (2023), "Effects of hygrothermal ageing and temperature on the mechanical behavior of aluminum-CFRP hybrid (riveted/bonded) joints", *Int. J. Adhes. Adhesiv.*, **121**, 103299. https://doi.org/10.1016/j.ijadhadh.2022.103299.

AP